Cellular/Molecular

Structural and Functional Plasticity of Astrocyte Processes and Dendritic Spine Interactions

Alberto Perez-Alvarez,[1,2]* Marta Navarrete,[1]* Ana Covelo,[4] Eduardo D. Martin,[3] and Alfonso Araque[1,4]

[1]Instituto Cajal, CSIC, 28002 Madrid, Spain, [2]Institute for Synaptic Physiology, Center for Molecular Neurobiology Hamburg (ZMNH), University Medical Center Hamburg-Eppendorf, 20251 Hamburg, Germany, [3]Laboratory of Neurophysiology and Synaptic Plasticity, Albacete Science and Technology Park (PCYTA), Institute for Research in Neurological Disabilities (IDINE), University of Castilla-La Mancha, 02006 Albacete, Spain, and [4]Department of Neuroscience, University of Minnesota, Minneapolis, Minnesota 55455

Experience-dependent plasticity of synaptic transmission, which represents the cellular basis of learning, is accompanied by morphological changes in dendritic spines. Astrocytic processes are intimately associated with synapses, structurally enwrapping and functionally interacting with dendritic spines and synaptic terminals by responding to neurotransmitters and by releasing gliotransmitters that regulate synaptic function. While studies on structural synaptic plasticity have focused on neuronal elements, the structural–functional plasticity of astrocyte–neuron relationships remains poorly known. Here we show that stimuli inducing hippocampal synaptic LTP enhance the motility of synapse-associated astrocytic processes. This motility increase is relatively rapid, starting <5 min after the stimulus, and reaching a maximum in 20–30 min ($t_{(1/2)} = 10.7$ min). It depends on presynaptic activity and requires G-protein-mediated Ca^{2+} elevations in astrocytes. The structural remodeling is accompanied by changes in the ability of astrocytes to regulate synaptic transmission. Sensory stimuli that increase astrocyte Ca^{2+} also induce similar plasticity in mouse somatosensory cortex *in vivo*. Therefore, structural relationships between astrocytic processes and dendritic spines undergo activity-dependent changes with metaplasticity consequences on synaptic regulation. These results reveal novel forms of synaptic plasticity based on structural–functional changes of astrocyte–neuron interactions.

Key words: **astrocyte; astrocyte–neuron interactions; dendritic spines; remodeling**

Introduction

Experience-induced plasticity of synaptic transmission, which represents the cellular basis of learning, is associated with morphological changes in synapses. Alterations in spine size as well as in density are thought to reflect changes in the strength of synaptic transmission (Maletic-Savatic et al., 1999; Toni et al., 1999; Wilbrecht et al., 2010). Astrocytes are emerging as key regulatory elements involved in synaptic function. They are intimately associated with synapses both structurally through the astrocytic processes that enwrap dendritic spines and presynaptic terminals (Haber et al., 2006; Theodosis et al., 2008), and functionally through their ability to respond to neurotransmitters and release gliotransmitters that modulate synaptic transmission (Volterra and Meldolesi, 2005; Perea et al., 2009; Halassa and Haydon, 2010; Araque et al., 2014). While studies on experience-dependent structural synaptic plasticity have mainly focused on neuronal structures (Lendvai et al., 2000; Yuste and Bonhoeffer, 2004; Holtmaat and Svoboda, 2009), the structural–functional plasticity of astrocyte–neuron relationships and their activity-dependent plasticity are poorly known.

We investigated whether structural relationships between astrocytic processes and dendritic spines undergo activity-dependent plasticity and analyzed the consequences on the astrocyte-induced regulation of synaptic transmission to determine the functional metaplasticity consequences of the structural changes in astrocytic processes at synapses. We found that stimuli that induce long-term potentiation and astrocyte Ca^{2+} signaling *in vitro* and *in vivo* enhance astrocytic process motility, a phenomenon that depends on presynaptic activity and requires G-protein-mediated Ca^{2+} elevations in astrocytes. This experience-dependent structural remodeling is accompanied by functional changes in the ability of astrocytes to regulate synaptic transmission. Present results reveal a novel form of experience-dependent plasticity based on dynamic structural–functional changes of astrocyte–neuron interactions.

Materials and Methods

All the procedures for handling and killing animals followed the European Commission guidelines (86/609/CEE).

Received June 11, 2014; revised Aug. 3, 2014; accepted Aug. 8, 2014.

Author contributions: A.P.-A., M.N., E.D.M., and A.A. designed research; A.P.-A., M.N., A.C., and E.D.M. performed research; A.P.-A., M.N., and A.C. analyzed data; A.P.-A., M.N., E.D.M., and A.A. wrote the paper.

This work was supported by grants from MINECO (BFU2010-15832, CSD2010-00045) and Cajal Blue Brain (to A.A.), MINECO (BFU2011-26339) and INCRECyT project from European Social Fund, JCCM, and PCyTA (to E.D.M.). A.P.-A. is a recipient of a Long Term EMBO Fellowship. We thank G. Perea and R. Gómez for helpful comments and B. Pro for technical assistance.

*A.P.-A. and M.N. contributed equally to this work.

The authors declare no competing financial interests.

Correspondence should be addressed to Dr. Alfonso Araque, Department of Neuroscience, University of Minnesota, 6-145 Jackson Hall, 321 Church Street SE, Minneapolis, MN 55455. E-mail: araque@umn.edu.

M. Navarrete's present address: Department of Neurobiology, Centro de Biología Molecular "Severo Ochoa" (CSIC)/Universidad Autónoma de Madrid (UAM), 28002 Madrid, Spain.

DOI:10.1523/JNEUROSCI.2401-14.2014

 0270-6474/14/3412738-07$15.00/0

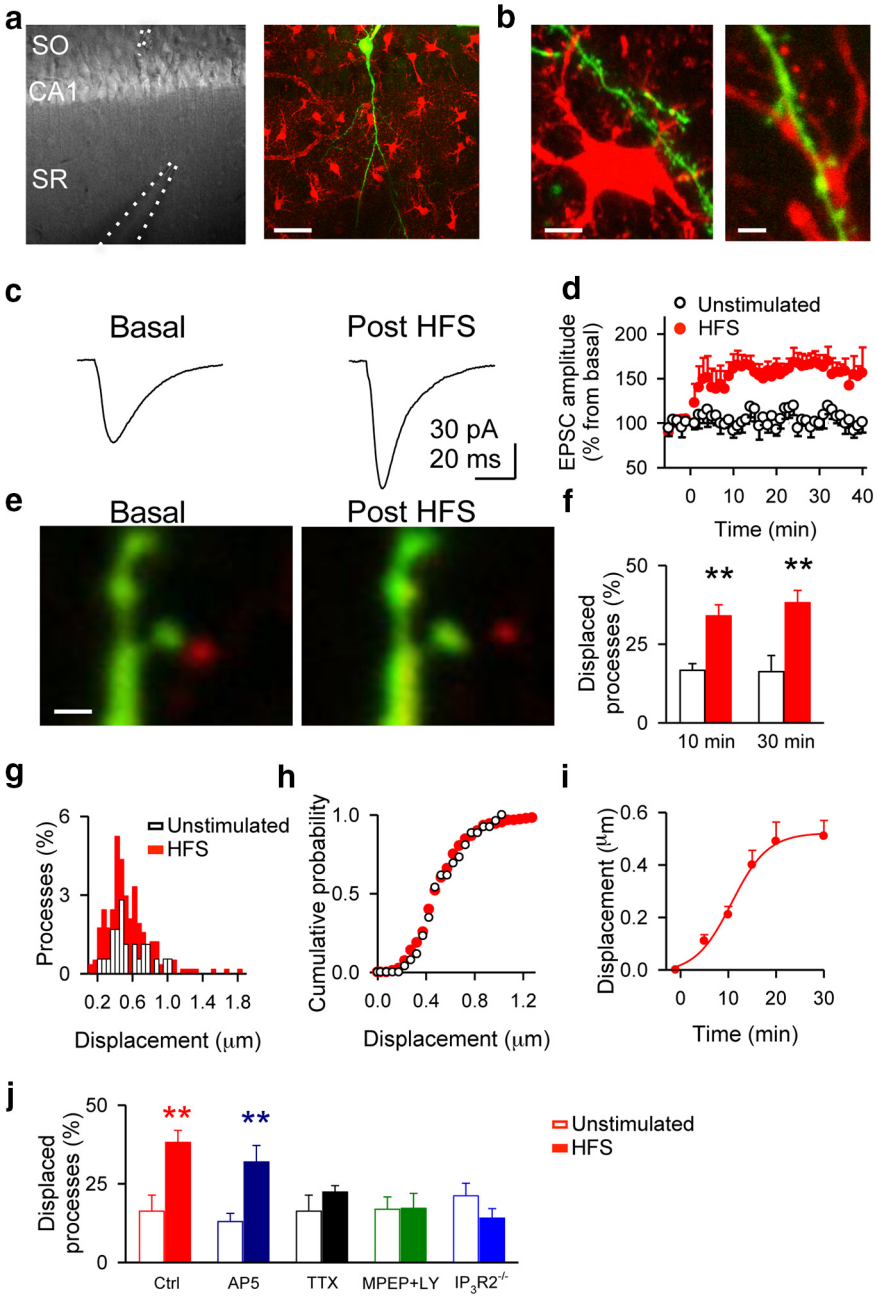

Figure 1. Synaptic transmission plasticity correlates with astrocytic process remodeling. ***a***, Left, Infrared image showing the recorded pyramidal neuron and stimulation electrode. Right, Alexa Fluor 488-filled neuron (green) and stratum radiatum astrocytes stained with SR101 (red). Scale bar, 40 μm. ***b***, Dendritic spines (green) and astrocytic processes (red). Scale bars: 5 and 2 μm, respectively. ***c***, EPSCs before and 30 min after delivering a HFS protocol. ***d***, Relative EPSC amplitudes in unstimulated ($n = 6$) and HFS ($n = 7$) slices. Zero time corresponds to the onset of the HFS protocol. ***e***, Astrocytic process (red) remodeling in the surrounding of excitatory synapses (green) after plasticity induction. Scale bar, 1 μm. ***f***, Average relative changes of displaced processes ($n = 6$ unstimulated, white bars; $n = 28$, HFS, red bars). ***g***, ***h***, Displacement amplitude histograms (bin width: 0.05 μm) and corresponding cumulative probability plots showing the percentage and distance traveled by astrocytic processes in unstimulated ($n = 5$) and HFS-stimulated ($n = 22$) slices at $t = 30$ min. ***i***, Time-lapse changes in astrocytic process position after induction of plasticity ($n = 5$). ***j***, Relative changes of displaced processes in control ($n = 7$), AP5 ($n = 5$), TTX ($n = 5$), MPEP + LY367385 ($n = 5$), and IP$_3$R2$^{-/-}$ mice ($n = 6$). Significant differences were established at $^{**}p < 0.01$.

Hippocampal slice preparation. Hippocampal slices (350–400 μm thick) were obtained from 13- to 18-d-old C57BL/6 wild-type, IP3R2$^{-/-}$ (generously donated by Dr. J Chen; Li et al., 2005) and Thy-1 GFP mice of either sex, as described previously (Araque et al., 2002). Slices were superfused with gassed (95% O_2/5% CO_2) artificial CSF that contained the following (in mM): 124 NaCl, 2.69 KCl, 1.25 KH_2PO_4, 2 $MgSO_4$, 26 $NaHCO_3$, 2 $CaCl_2$, and 10 glucose 10, pH 7.3, and included 0.05 mM picrotoxin and 5 mM CGP55845 to block GABA receptors.

In vivo *preparation.* Four to 12-week-old mice of either sex were prepared as previously described (Pérez-Alvarez et al., 2013). A cranial window over the somatosensory cortex (−1 mm posterior to bregma and 3.4 mm lateral from midline) was performed. Stimulation of the contralateral whisker pad was achieved applying 100 ms air puffs with a capillary glass. Trains of 150 puffs (5 Hz) were delivered with an interval of 30 s for 5 min. Simultaneously, the tail was pinched with steel forceps at 2 Hz.

Imaging. Animals were injected intraperitoneally with SR101 (100 mg/kg) 2 h before imaging. An Olympus FV300 laser-scanning confocal microscope was used, as detailed previously (Pérez-Alvarez et al., 2013). Apical dendrites of CA1 pyramidal neurons were imaged in slices including 40 μM Alexa Fluor 488 sodium hydrazide in the recording intracellular solution. *In vivo*, apical dendrites from layer V pyramidal neurons expressing eGFP were imaged. The dendritic tree and its spines were used as a reference of synaptic structure. Ca^{2+} levels in astrocytes were monitored using the Ca^{2+} indicator Fluo-4 AM (1 μg/μl) dissolved in HEPES-buffered saline containing 1% pluronic. Image acquisition rate was 1–2 Hz.

Electrophysiology. Whole-cell recordings from CA1 pyramidal neurons were performed in slices, as detailed previously (Navarrete et al., 2012). The HFS protocol consisted in four trains at 5 Hz of five stimuli at 40 Hz delivered 10 times at 0.1 Hz. The spike timing-dependent plasticity (STDP) protocol was performed in current-clamp, and EPSPs (1 Hz) were paired (10 ms delay) with action potentials evoked by 3 ms, 1–2 nA current pulses. For i*n vivo*, a monopolar electrode was placed in the barrel-field region (−1 mm posterior to bregma, 3.4 mm lateral from midline, and depth of 50–200 μm below the brain surface) to record the local field potential (LFP). LFP was evoked by stimulation of contralateral whisker pad, which was elicited by two nichrome subcutaneous electrodes (insulated except at the tips) located at the dorsoanterior and caudoposterior edges of the whisker pad.

For statistical analysis we used the Student's *t* test for normally distributed data or Mann–Whitney as nonparametric test. Statistical significance was assessed at $p < 0.05$. Error bars in figures indicate SEM.

Results

Synaptic transmission plasticity induces astrocytic process remodeling

We first monitored the morphological dynamics of astrocytic processes associated with dendritic spines in mice hippocampal slices. We intravitally labeled astrocytes with sulforhodamine 101 (SR101; Nimmerjahn et al., 2004; Pérez-Alvarez et al., 2013) and recorded Schaffer collateral (SC)-evoked EPSCs from CA1 pyramidal neurons loaded with Alexa Fluor 488 through the patch pipette (Fig. 1*a*,*b*).

We quantified the motility of peridendritic astrocytic processes (PDAPs) adjacent (<5 μm from the reference dendritic

axes) to dendritic spines before and after stimulating SC with a train of HFS, which evoked LTP of synaptic transmission (154.0 ± 18.6%; $n = 7$, $p < 0.01$; Fig. 1*c*,*d*). The percentage of PDAPs that showed a displacement (>0.125 μm from their initial location) was significantly enhanced 10 and 30 min after HFS (34.0 ± 3.5 and 38.2 ± 3.9%, respectively; 884 PDAPs, $n = 28$ slices) when compared with unstimulated conditions (16.7 ± 2.1 and 16.3 ± 5.1%; 283 PDAPs, $n = 6$ slices; $p < 0.01$; Fig. 1*e*,*f*). This overall motility increase of PDAPs induced after HFS was not associated with longer displacements of particular processes but with the number of moving PDAPs (mean displacements of PDAPs at 30 min were 0.65 ± 0.10 and 0.55 ± 0.02 μm in unstimulated conditions and after HFS; $n = 27$ and $n = 208$, 5 and 22 slices, respectively, $p = 0.94$; Fig. 1*g*,*h*). Of 338 astrocytic processes that showed displacement after HFS, 74% moved away, 14% approached, and 13% moved along the reference neuronal element. The time course of the mean displacements of astrocyte processes after HFS could be fitted to a Boltzmann equation ($D_{max} = 0.55$ μm, slope = 3.8, $n = 5$; Fig. 1*i*). Significant displacements occurred as fast as 5 min after HFS, they reached a maximum between 20 and 30 min, and the time at which half of the mean displacements occurred was $t_{(1/2)} = 10.7$ min. These results indicate that the motility increase of PDAPs induced by HFS was a relatively rapid phenomenon that saturated over time.

We then investigated the cellular origin of the signals involved in the increase in PDAP motility. The enhanced motility was unaffected by the NMDA receptor antagonist D-AP5 (50 μM; 264 PDAPs, $n = 5$ slices; $p < 0.01$; Fig. 1*j*), but was absent in the presence of 1 μM TTX (224 PDAPs, $n = 5$ slices, $p = 0.33$; Fig. 1*j*), indicating that this phenomenon does not require the postsynaptic expression of LTP but depends on presynaptic activity.

Astrocytes sense glutamatergic activity through activation of astrocytic mGluR, which elevates astrocyte Ca^{2+} (Porter and McCarthy, 1996; Perea and Araque, 2005, 2007; Panatier et al., 2011). Group I mGluR antagonists (MPEP 50 μM and LY367385 100 μM) prevented the PDAP motility increase (165 PDAPs, $n = 5$ slices, $p = 0.98$; Fig. 1*j*) without affecting the HFS-induced LTP (180.0 ± 25.6%; $n = 4$, $p < 0.05$), suggesting that glutamate released during HFS enhanced PDAP motility through activation of astrocytic mGluRs. We then tested whether the astrocyte Ca^{2+} signal induced by activation of mGluRs was necessary to increase PDAP motility using IP_3-receptor type 2-deficient mice ($IP_3R2^{-/-}$), in which G-protein-mediated Ca^{2+} mobilization is impaired in astrocytes (Petravicz et al., 2008; Di Castro et al., 2011; Navarrete et al., 2012). The activity-dependent PDAP motility enhancement was absent in slices from $IP_3R2^{-/-}$ mice (264 PDAPs, $n = 6$ slices, $p = 0.19$; Fig. 1*j*). These results indicate that PDAP motility was controlled by presynaptic activity, activation of astrocytic mGluRs, and astrocyte Ca^{2+} elevations.

LTP induced by STDP correlates with astrocytic process remodeling

We then asked whether PDAP motility was also sensitive to other induction paradigms of synaptic plasticity. We used an STDP paradigm consisting in pairing presynaptic stimuli with postsynaptic action potentials (Markram et al., 1997), while monitoring PDAP movement. The STDP-induced LTP (186.5 ± 12.4%; $n = 5$, $p < 0.01$; Fig. 2*a*,*b*) was accompanied by an enhancement of the proportion of PDAPs displaced from the original location compared with unstimulated slices (32.7 ± 8.2 and 16.7 ± 2.1%, respectively, at 10 min; and 38.6 ± 7.8 and 16.3 ± 5.1%, respectively, at 30 min; 117 and 283 PDAPs, $n = 5$ and $n = 6$ slices, respectively, $p < 0.05$; Fig. 2*c*,*d*). The increase in the proportion of displaced PDAPs was therefore similar after inducing synaptic plasticity with STDP or HFS paradigms (38.6 ± 7.8 and 38.2 ± 3.9% at 30 min; 117 and 884 PDAPs, $n = 5$ and $n = 28$ slices, respectively, $p = 0.96$). Moreover, the STDP-induced enhancement of PDAP motility was also absent in $IP_3R2^{-/-}$ mice (21.2 ± 4.0 and 14.1 ± 3.0% unstimulated and STDP stimulated slices at 30 min; 264 and 123 PDAPs, $n = 6$ and $n = 5$ slices, respectively, $p = 0.19$; Fig. 2*e*,*f*), indicating that this phenomenon requires astrocyte Ca^{2+} mobilization from internal stores. These results indicate that PDAP motility enhancement associated with synaptic plasticity is a general phenomenon that does not depend on specific stimulus paradigms.

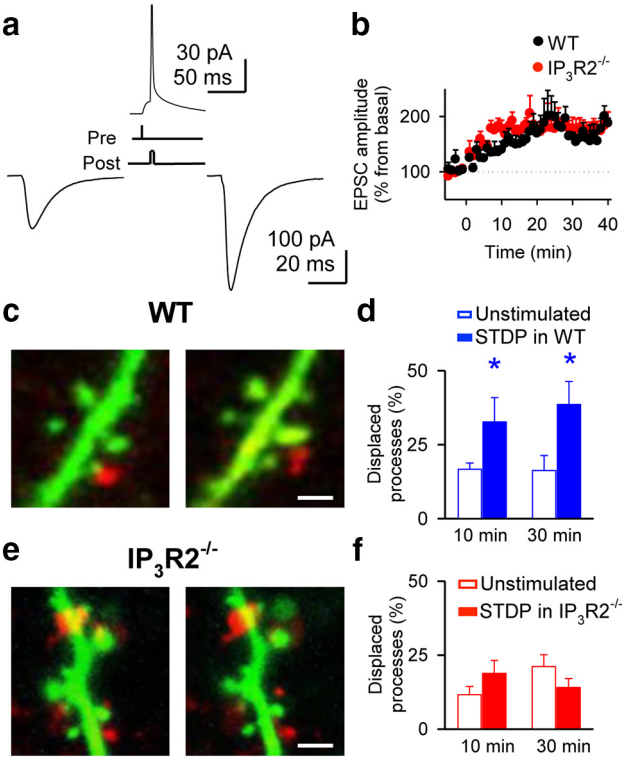

Figure 2. STDP correlates with astrocytic process remodeling. ***a***, EPSCs before (left) and 30 min after (right) STDP protocol (top). ***b***, Relative EPSC amplitudes in slices from wild-type (WT; $n = 5$) and $IP_3R2^{-/-}$ ($n = 6$) mice. Zero time corresponds to the onset of the STDP protocol. ***c***, Dendritic spines (green) and astrocytic processes (red) before (left) and 30 min after (right) delivering the STDP protocol in wild-type mice. Scale bar, 1 μm. ***d***, Quantification of displaced processes in unstimulated ($n = 6$) and STDP-stimulated ($n = 5$) slices from wild-type mice. ***e***, ***f***, As in ***c***, ***d***, respectively, but in slices from $IP_3R2^{-/-}$ mice. Scale bar, 2 μm. Significant differences were established at $^*p < 0.05$.

Synaptic transmission is modulated by the activity-dependent motility of astrocytic PDAPs

We next investigated whether the activity-dependent motility of PDAPs resulted in changes in astrocytic ability to modulate synaptic transmission. We used an experimental paradigm known to induce astrocyte-mediated synaptic modulation, i.e., endocannabinoids (ECBs) released from depolarized neurons stimulate the astrocyte Ca^{2+} signal that leads to a transient enhancement of synaptic efficacy at single CA3–CA1 synapses (Navarrete and Araque, 2008, 2010). We performed paired recordings from CA1 pyramidal neurons, monitored astrocyte Ca^{2+}, and stimulated SC using the minimal stimulation technique that activates single presynaptic fibers (Dobrunz and Stevens, 1997; Perea and Araque, 2007; Navarrete and Araque, 2010; Navarrete et al.,

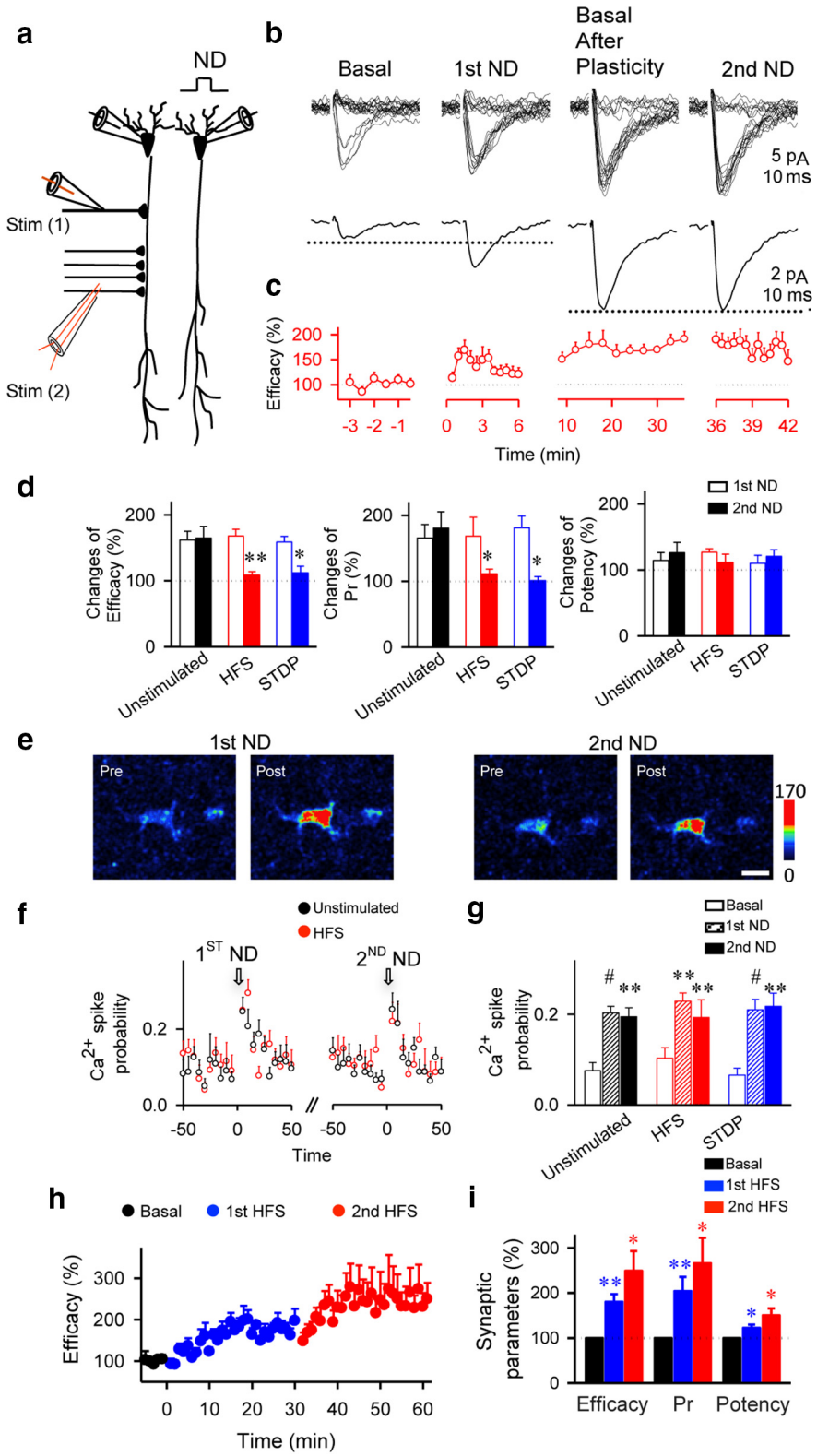

Figure 3. Astrocytic modulation of synaptic transmission is impaired after LTP protocol. ***a***, Scheme of paired-recorded pyramidal neurons and the stimulating electrodes. ***b***, Responses evoked by minimal stimulation (top traces) and average EPSCs ($n = 60$ stimuli, including successes and failures; bottom traces) before (basal), after first ND, 30 min after HFS (Basal After Plasticity), and after second ND. ***c***, Synaptic efficacy (i.e., mean amplitude of responses including successes and failures of neurotransmission) before, after first ND, 30 min after HFS, and after second ND ($n = 7$). First and second NDs were delivered at 0 and 36 min, respectively. ***d***, Relative changes from control basal values of synaptic parameters after first and second ND in unstimulated ($n = 7$), HFS ($n = 7$), and STDP ($n = 5$)-stimulated slices. Pr, Probability of release. ***e***, Fluorescence intensities of Fluo-4-filled astrocytes before and after first and second ND. Scale bar, 10 μm. ***f***, Astrocyte Ca^{2+} spike probability in unstimulated (111 astrocytes, $n = 11$ slices) and HFS conditions (71 astrocytes, $n = 8$ slices). Zero time corresponds to the beginning of ND. ***g***, Ca^{2+} spike probability before (basal; white bars) and after first (striped bars) and second ND ($n = 5$; filled bars) in unstimulated ($n = 11$) and HFS ($n = 8$) or STDP ($n = 6$)-stimulated. ***h***, Relative synaptic efficacy evoked by minimal stimulation versus time before (basal, black circles), after first stimuli (first HFS, blue circles), and after second stimuli (second HFS, red circles; $n = 4$). Zero time corresponds to the onset of first HFS. Note that the system is not saturated after first stimulation. ***i***, Relative changes from control values (basal, black bars) of synaptic parameters after first (blue bars) and second (red bars) HFS ($n = 4$). Significant differences were established at $^{*}p < 0.05$, $^{**}p < 0.01$, and $\#p < 0.001$.

2012). We depolarized one pyramidal neuron (to 0 mV for 5 s) to stimulate ECB release and monitored synaptic transmission parameters at synapses in the other neuron (Navarrete and Araque, 2010). We applied a first neuronal depolarization (first ND) to assess that the recorded synapses showed the transient ECB-induced, astrocyte-mediated synaptic potentiation. We then applied the HFS paradigm to induce LTP, and 30 min after the LTP induction we applied a second ND to test whether the astrocyte-induced synaptic modulation was altered (Fig. 3). In the absence of HFS, the transient enhancement of synaptic efficacy evoked by the first ND (delivered at the beginning of the recordings) was similar to that evoked by the second ND (delivered 30 min later; mean transient potentiations of synaptic efficacy were 161.7 ± 13.2% for first ND and 165.0 ± 17.7% for second ND from basal values; $n = 7$). In contrast, the astrocyte-mediated, synaptic efficacy enhancement induced by the first ND was not reproduced by the second ND delivered 30 min after inducing LTP with either HFS (167.8 ± 10.2 vs 108.4 ± 5.3%) or STDP (158.7 ± 5.3 vs 112.0 ± 10.0%, $n = 7$ and $n = 5$, $p < 0.01$ and $p < 0.05$, respectively; Fig. 3*b–d*). Similar astrocyte Ca^{2+} signals were evoked by the first and second NDs (111 astrocytes from $n = 11$ unstimulated slices and 71 astrocytes from $n = 8$ HFS slices, $p < 0.01$; Fig. 3*e–g*), indicating that differences in the astrocyte-induced synaptic modulation are mediated by plastic changes of regulatory mechanisms downstream the astrocyte Ca^{2+} signal. Furthermore, the failure of the second ND to induce synaptic potentiation was not due to a saturation of LTP mechanisms, because stimulating synapses with a second train of HFS delivered 30 min after inducing LTP with an initial train could still further enhance the synaptic efficacy (synaptic efficacy potentiation from basal: 180.6 ± 16.8% for first HFS and 249.4 ± 43.6% for second HFS; $n = 4$, $p < 0.01$ and $p < 0.05$, respectively;

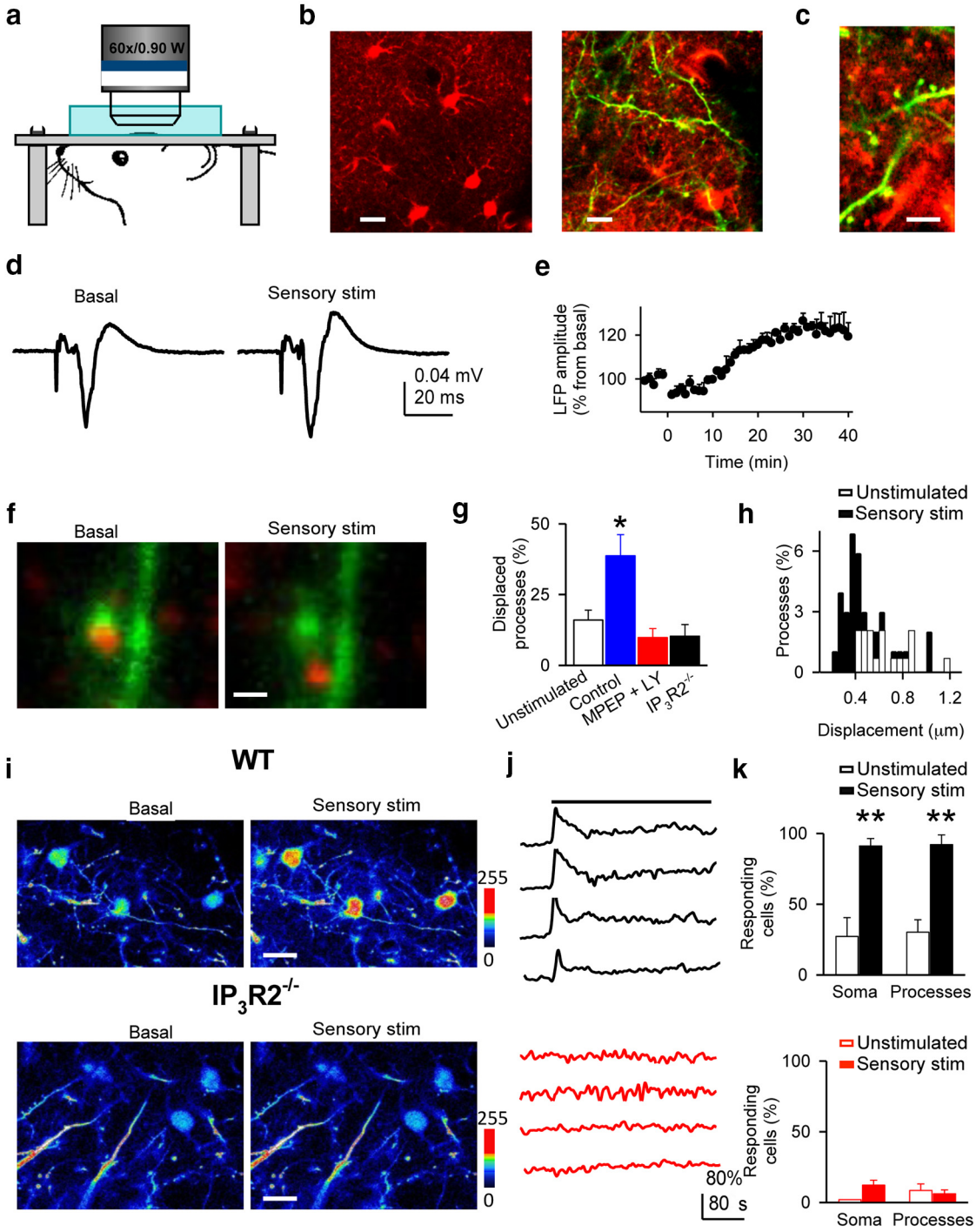

Figure 4. *In vivo* sensory stimulation correlates with astrocytic process remodeling in primary somatosensory cortex. ***a***, Scheme of the *in vivo* imaging. ***b***, ***c***, Images at different magnification of *in vivo* astrocytes and processes stained with SR101 (red) and dendrites (green). Scale bars: ***b***, left, 10 μm; right, 5 μm; ***c***, 2 μm. ***d***, LFP responses to whisker stimulation before and after sensory stimulation. ***e***, Relative LFP responses ($n = 5$) before and after sensory stimulation at $t = 0$. ***f***, Representative example of *in vivo* astrocytic process displacement after sensory stimulation. Scale bar, 1 μm. ***g***, Displaced processes 30 min after sensory stimulation in unstimulated ($n = 4$), and stimulated in control ($n = 4$), MPEP + LY367385 ($n = 8$), and in the $IP_3R2^{-/-}$ mice ($n = 4$). ***h***, Displacement amplitude histograms (bin width: 0.05 μm) of *in vivo* astrocytic processes in unstimulated and sensory-stimulated mice ($t = 30$ min). ***i***, *In vivo* images of Fluo-4-filled astrocytes before and after sensory stimulation from wild-type and $IP_3R2^{-/-}$ mice. Scale bar, 10 μm. ***j***, Ca^{2+} levels from four astrocytes from wild-type (black traces) and $IP_3R2^{-/-}$ mice (red traces). Horizontal bar indicates sensory stimulation. ***k***, Responding astrocytes from wild-type (top; 85 astrocytes, $n = 4$ mice) and $IP_3R2^{-/-}$ mice (bottom; 67 astrocytes, $n = 3$ mice) in unstimulated and sensory stimulation conditions. Significant differences were established at $^*p < 0.05$, $^{**}p < 0.01$.

Fig. 3*h*,*i*). Therefore, the astrocyte ability to regulate synaptic transmission was impaired after inducing LTP, suggesting that consolidated synapses that experienced synaptic plasticity were less sensitive to astrocyte regulation.

In vivo sensory stimulation correlates with astrocytic process remodeling

We investigated whether activity-dependent plasticity of structural interactions between astrocyte processes and dendritic

spines occurs upon sensory stimulation in primary somatosensory cortex *in vivo*. We simultaneously monitored SR101-stained PDAPs (Pérez-Alvarez et al., 2013) and dendritic spines in Thy1-eGFP-M mice (Feng et al., 2000; Pérez-Alvarez et al., 2013), as well as astrocyte Ca^{2+}. We first confirmed that sensory stimulation induced LTP in layer V of primary somatosensory cortex (Takata et al., 2011; 119 ± 3.4%; $n = 5$, $p < 0.05$; Fig. 4*a–e*). Sensory stimulation significantly enhanced the proportion of PDAPs that showed a displacement from their original position when compared with unstimulated animals (38.7 ± 7.5 and 12.9 ± 4.1% at 30 min; 103 and 145 PDAPs, $n = 4$ and $n = 6$ mice, respectively, $p < 0.05$; Fig. 4*f–h*). A few astrocytes from $IP_3R2^{-/-}$ mice responded with small calcium elevations at the soma (9 of 67 astrocytes showed $\Delta F = 8 \pm 2\%$, whereas in wild-type mice 77 of 85 astrocytes showed $\Delta F = 142 \pm 10\%$), suggesting additional IP_3R2-independent mechanisms underlying Ca^{2+} elevations but with relatively minor contribution (Shigetomi et al., 2013). It also transiently increased intracellular Ca^{2+} levels in astrocytic somas (Wang et al., 2006; Navarrete et al., 2012) as well as in processes in Thy1-eGFP-M mice (85 astrocytes, $n = 4$ mice, $p < 0.001$), but failed to induce Ca^{2+} changes in $IP_3R2^{-/-} \times$ Thy1-eGFP-M mice (67 astrocytes, $n = 3$ mice, $p = 0.23$; Fig. 4*i–k*). Consistent with results obtained in slices, PDAP motility increase was prevented by the group I mGluR antagonists MPEP + LY367385 (5 mg/kg, i.p. injected; 176 PDAPs, $n = 8$ mice, $p = 0.24$) and was absent in $IP_3R2^{-/-}$xThy1-eGFP-M mice (90 PDAPs, $n = 4$ mice, $p = 0.66$; Fig. 4*g*), indicating that sensory stimulation-induced PDAP motility increase depends on mGluR activation and requires astrocyte Ca^{2+} elevations. These results indicate that structural arrangement between astrocyte processes and dendritic spines undergo activity-dependent plasticity *in vivo*. Furthermore, the fact that this plasticity was observed in adult animals indicates that it is not exclusively a developmental phenomenon but that it may also serve as a cellular mechanism underlying learning and memory.

Discussion

Our results show that structural relationships between dendritic spines and astrocytic processes are activity-dependent regulated, and are associated with synaptic plasticity phenomena accompanied by metaplasticity consequences on the astrocytic regulation of synaptic transmission. This phenomenon does not depend on postsynaptic expression of synaptic plasticity but requires presynaptic activity, mGluR activation, and astrocyte Ca^{2+} signaling. These structural changes might account for the observed changes in the synaptic regulation by astrocytes; however, present findings do not provide evidence for a direct causal relationship of both phenomena and alternative mechanisms might be involved.

The coverage of synapses by astrocytic processes may change under different physiological conditions (Theodosis et al., 2008; Tanaka et al., 2013). 3D reconstructions of the hippocampal neuropil have shown that astrocyte coverage is higher in thin spines than in larger spines (Medvedev et al., 2014). Other studies have shown that a subset of synapses in stimulated brain areas appear to have a greater ability to attract astrocytic membrane, possibly reflecting enhanced neuronal activity and adaptation of glutamate uptake (Lushnikova et al., 2009). A more recent report showed that astrocytes actively engulf and phagocytose weak synapses in the retinogeniculate system, participating in synapse remodeling and neural circuit refinement (Chung et al., 2013). Our results provide further evidence of morphological changes of astrocytic processes, revealing that such dynamic phenomena (1) occur in a relatively fast temporal scale, (2) are controlled by synaptic plasticity events, and (3) may in turn, alter the astrocytic impact on synaptic efficacy.

Present findings showing plasticity of the structural and functional relationships between astrocytic processes and dendritic spines expand the idea that changes of neuronal elements represent the cellular basis of learning, including astrocyte processes as additional elements underlying experience-induced plasticity. Our results reveal an additional mechanism with relevant consequences in refining the structural and functional connectivity of the brain during development as well as in learning and memory.

References

Araque A, Martín ED, Perea G, Arellano JI, Buño W (2002) Synaptically released acetylcholine evokes Ca2+ elevations in astrocytes in hippocampal slices. J Neurosci 22:2443–2450. Medline

Araque A, Carmignoto G, Haydon PG, Oliet SH, Robitaille R, Volterra A (2014) Gliotransmitters travel in time and space. Neuron 81:728–739. CrossRef Medline

Chung WS, Clarke LE, Wang GX, Stafford BK, Sher A, Chakraborty C, Joung J, Foo LC, Thompson A, Chen C, Smith SJ, Barres BA (2013) Astrocytes mediate synapse elimination through MEGF10 and MERTK pathways. Nature 504:394–400. CrossRef Medline

Di Castro MA, Chuquet J, Liaudet N, Bhaukaurally K, Santello M, Bouvier D, Tiret P, Volterra A (2011) Local Ca2+ detection and modulation of synaptic release by astrocytes. Nat Neurosci 14:1276–1284. CrossRef Medline

Dobrunz LE, Stevens CF (1997) Heterogeneity of release probability, facilitation, and depletion at central synapses. Neuron 18:995–1008. CrossRef Medline

Feng G, Mellor RH, Bernstein M, Keller-Peck C, Nguyen QT, Wallace M, Nerbonne JM, Lichtman JW, Sanes JR (2000) Imaging neuronal subsets in transgenic mice expressing multiple spectral variants of GFP. Neuron 28:41–51. CrossRef Medline

Haber M, Zhou L, Murai KK (2006) Cooperative astrocyte and dendritic spine dynamics at hippocampal excitatory synapses. J Neurosci 26:8881–8891. CrossRef Medline

Halassa MM, Haydon PG (2010) Integrated brain circuits: astrocytic networks modulate neuronal activity and behavior. Annu Rev Physiol 72:335–355. CrossRef

Holtmaat A, Svoboda K (2009) Experience-dependent structural synaptic plasticity in the mammalian brain. Nat Rev Neurosci 10:647–658. CrossRef Medline

Lendvai B, Stern EA, Chen B, Svoboda K (2000) Experience-dependent plasticity of dendritic spines in the developing rat barrel cortex in vivo. Nature 404:876–881. CrossRef Medline

Li X, Zima AV, Sheikh F, Blatter LA, Chen J (2005) Endothelin-1-induced arrhythmogenic Ca2+ signaling is abolished in atrial myocytes of inositol-1,4,5-trisphosphate(IP3)-receptor type 2-deficient mice. Circ Res 96:1274–1281. CrossRef Medline

Lushnikova I, Skibo G, Muller D, Nikonenko I (2009) Synaptic potentiation induces increased glial coverage of excitatory synapses in CA1 hippocampus. Hippocampus 19:753–762. CrossRef Medline

Maletic-Savatic M, Malinow R, Svoboda K (1999) Rapid dendritic morphogenesis in CA1 hippocampal dendrites induced by synaptic activity. Science 283:1923–1927. CrossRef Medline

Markram H, Lübke J, Frotscher M, Sakmann B (1997) Regulation of synaptic efficacy by coincidence of postsynaptic APs and EPSPs. Science 275:213–215. CrossRef Medline

Medvedev N, Popov V, Henneberger C, Kraev I, Rusakov DA, Stewart MG (2014) Glia selectively approach synapses on thin dendritic spines. Philos Trans R Soc B, in press.

Navarrete M, Araque A (2008) Endocannabinoids mediate neuron-astrocyte communication. Neuron 57:883–893. CrossRef Medline

Navarrete M, Araque A (2010) Endocannabinoids potentiate synaptic transmission through stimulation of astrocytes. Neuron 68:113–126. CrossRef Medline

Navarrete M, Perea G, Fernandez de Sevilla D, Gómez-Gonzalo M, Núñez A, Martin ED, Araque A (2012) Astrocytes mediate in vivo cholinergic-induced synaptic plasticity. PLoS Biol 10:e1001259. CrossRef Medline

Nimmerjahn A, Kirchhoff F, Kerr JN, Helmchen F (2004) Sulforhodamine

101 as a specific marker of astroglia in the neocortex in vivo. Nat Methods 1:31–37. CrossRef Medline

Panatier A, Vallée J, Haber M, Murai KK, Lacaille JC, Robitaille R (2011) Astrocytes are endogenous regulators of basal transmission at central synapses. Cell 146:785–798. CrossRef Medline

Perea G, Araque A (2005) Properties of synaptically evoked astrocyte calcium signal reveal synaptic information processing by astrocytes. J Neurosci 25:2192–2203. CrossRef Medline

Perea G, Araque A (2007) Astrocytes potentiate transmitter release at single hippocampal synapses. Science 317:1083–1086. CrossRef Medline

Perea G, Navarrete M, Araque A (2009) Tripartite synapses: astrocytes process and control synaptic information. Trends Neurosci 32:421–431. CrossRef Medline

Pérez-Alvarez A, Araque A, Martín ED (2013) Confocal microscopy for astrocyte in vivo imaging: recycle and reuse in microscopy. Front Cell Neurosci 7:51. CrossRef Medline

Petravicz J, Fiacco TA, McCarthy KD (2008) Loss of IP3 receptor-dependent Ca2+ increases in hippocampal astrocytes does not affect baseline CA1 pyramidal neuron synaptic activity. J Neurosci 28:4967–4973. CrossRef Medline

Porter JT, McCarthy KD (1996) Hippocampal astrocytes in situ respond to glutamate released from synaptic terminals. J Neurosci 16:5073–5081. Medline

Shigetomi E, Jackson-Weaver O, Huckstepp RT, O'Dell TJ, Khakh BS (2013) TRPA1 channels are regulators of astrocyte basal calcium levels and long-term potentiation via constitutive D-serine release. J Neurosci 33:10143–10153. CrossRef Medline

Takata N, Mishima T, Hisatsune C, Nagai T, Ebisui E, Mikoshiba K, Hirase H (2011) Astrocyte calcium signaling transforms cholinergic modulation to cortical plasticity *in vivo*. J Neurosci 31:18155–18165. CrossRef Medline

Tanaka M, Shih PY, Gomi H, Yoshida T, Nakai J, Ando R, Furuichi T, Mikoshiba K, Semyanov A, Itohara S (2013) Astrocytic Ca2+ signals are required for the functional integrity of tripartite synapses. Mol Brain 6:6. CrossRef Medline

Theodosis DT, Poulain DA, Oliet SH (2008) Activity-dependent structural and functional plasticity of astrocyte-neuron interactions. Physiol Rev 88:983–1008. CrossRef Medline

Toni N, Buchs PA, Nikonenko I, Bron CR, Muller D (1999) LTP promotes formation of multiple spine synapses between a single axon terminal and a dendrite. Nature 402:421–425. CrossRef Medline

Volterra A, Meldolesi J (2005) Astrocytes, from brain glue to communication elements: the revolution continues. Nat Rev Neurosci 6:626–640. CrossRef Medline

Wang X, Lou N, Xu Q, Tian GF, Peng WG, Han X, Kang J, Takano T, Nedergaard M (2006) Astrocytic Ca2+ signaling evoked by sensory stimulation in vivo. Nat Neurosci 9:816–823. CrossRef Medline

Wilbrecht L, Holtmaat A, Wright N, Fox K, Svoboda K (2010) Structural plasticity underlies experience-dependent functional plasticity of cortical circuits. J Neurosci 30:4927–4932. CrossRef Medline

Yuste R, Bonhoeffer T (2004) Genesis of dendritic spines: insights from ultrastructural and imaging studies. Nat Rev Neurosci 5:24–34. CrossRef Medline